




Enhancements of thermal, electrical, and electromagnetic interference shielding properties of polybenzoxazine/1,5-naphthalene disulfonic acid-doped polypyrrole nanocomposites

Noureddine Ramdani^{1,*}, EL-Oualid Mokhnache¹, Mohammed Seddik Razali¹, Mokhtar Maamar¹, Hicham Mehras¹, Nacereddine Abid¹, and Mehdi Derradji^{1,*} 

¹ UER Procédés Energétiques, Ecole Militaire Polytechnique, BP 17, Bordj El Bahri, Algiers, Algeria

Received: 5 February 2023

Accepted: 30 August 2023

Published online:

14 September 2023

© The Author(s), under exclusive licence to Springer Science+Business Media, LLC, part of Springer Nature, 2023

ABSTRACT

In this study, a new series of 1,5-naphthalene disulfonic acid-doped polypyrrole (NDA.PPy)-filled polybenzoxazine nanocomposites were produced by a melt-mixing process. The effect of NDA.PPy ratio on the curing behavior, the microstructure, and the electrical conductivity, of these nanocomposites was evaluated by various techniques. The electromagnetic interference shielding effectiveness (EMI SE) of the developed nanocomposites in the X-band frequency range (8–12 GHz) was also studied in terms NDA.PPy ratios and the thickness of specimens. The thermal curing data showed that the addition of NDA.PPy positively catalyzed the curing process of benzoxazine monomer by decreasing its higher curing temperature and the enthalpy of cure. The higher aspect ratio and better dispersion of the NDA.PPy nanofillers resulted in a great improvement in the electrical conductivity for these nanocomposites compared to the unfilled matrix, where it increased from 1.24×10^{-14} to 22.3 S.cm^{-1} as the NDA.PPy loading changed from 0 to 30 wt%, respectively. Surprisingly, the presence of conductive NDA.PPy nanofillers into the polybenzoxazine matrix improved its shielding efficiency by absorption loss mechanism. Moreover, a total EMI SE of 27.2 (81% by absorption loss) and 46.4 dB (86% by absorption loss) were recorded for the 2- and 5-mm-thick nanocomposites filled with 30 wt% NDA.PPy, respectively. These findings indicate that the newly developed nanocomposites can meet the requirements of many industrial electromagnetic radiofrequency shielding applications by shielding more than 99.9% of incident radiation.

Address correspondence to E-mail: redwen_ramdani@yahoo.com; derradjimehdi1@gmail.com

1 Introduction

In our days, electromagnetic interference (EMI) has become a serious technological problem due to the fast development of electronic and telecommunication devices, which release harmful electromagnetic radiation and can disrupt the performance of electronic gadgets and provoke severe health problems for their users [1, 2]. To protect these electronics tools against EMI and improve their efficiencies and durability, extensive research has been directed toward producing EMI shielding or absorbing materials [3]. Polymer composites filled with various fillers, including 2D MXenes, metallic, ceramics, and carbon-based nanomaterials, have also been developed to ensure EMI shielding against both the low frequencies and the radiofrequencies [4–9]. The EMI shielding effectiveness is achieved through three main mechanisms known as reflection (SE_R), absorption (SE_A), and multiple reflections (SE_M) of the electromagnetic waves. Due to the increased demand for microwave absorbing materials, the attenuation of EMI by absorption mechanisms is preferred instead of reflection [10, 11].

In this regard, a wide range of electrically conductive polymer composites and nanocomposites based on intrinsically conducting conjugated polymers (ICP), such as polythiophene, polypyrrole (PPy), and polyaniline (PAni), have been developed for EMI shielding applications [12–14]. The focus on using these hybrid systems is attributed to their low densities, corrosion resistance, tailored electrical conductivity, design flexibility, ease of processing, high thermal stability, high electromagnetic interference shielding effectiveness (EMI SE), and higher microwave absorption characteristics [15, 16]. It has been reported that the EMI SE value in the range of 15 to 30 dB of the EMI radiation, corresponding to 99.9% attenuation, can meet the requirement of many applications [17]. It is also reported that the electrical conductivity of microwave absorbing materials must be varied between 10^{-4} and 10^{-1} S.cm⁻¹. Thus, it is thought that the addition of conjugated polymer particles such as PPy can be very suitable to satisfy this condition.

In the last two decades, polybenzoxazine thermoset, as a new generation of phenolic resin, has emerged as the most versatile and widely used engineering matrix for producing high-performance composite materials, because of its exceptional properties, such as no need for external hardener, its high glass transition temperature, improved adhesion properties, higher thermal

stability, good chemical resistance, low shrinkage upon cure, molecular design flexibility, and good barrier properties [18–21]. However, the need for a high curing temperature and brittleness is still the most serious problems related to benzoxazines monomers, while blending with other polymers, synthesizing of new flexible monomers, or developing their high-performance composites appear as promising solutions to overcome these shortcomings. On the other hand, some thermal and physical characteristics promote the usage of benzoxazine thermosets in a wide range of applications in various industries, like high-performance coatings, matrices for fiber-reinforced composites in aerospace, and microelectronic packaging [22].

Recently, polybenzoxazine-based nanocomposites with various conductive carbon-based nanofillers have been developed to provide specific electromagnetic interference (EMI) shielding and microwave absorbing properties [23–26]. However, to the best of our knowledge, no work has been reported on the electromagnetic shielding properties of polybenzoxazine/polypyrrole nanocomposites. In this work, new type of phenol-aniline-based polybenzoxazine filled with 1,5-naphthalene disulfonic acid-doped polypyrrole nanocomposites (Poly(P-a)/NDA.PPy) were produced by a melt-mixing process to evaluate the effect of NDA.PPy loading on the curing behavior, electrical properties, and electromagnetic shielding characteristics of polybenzoxazine matrix from 0 to 30 wt%.

2 Experimental

2.1 Materials

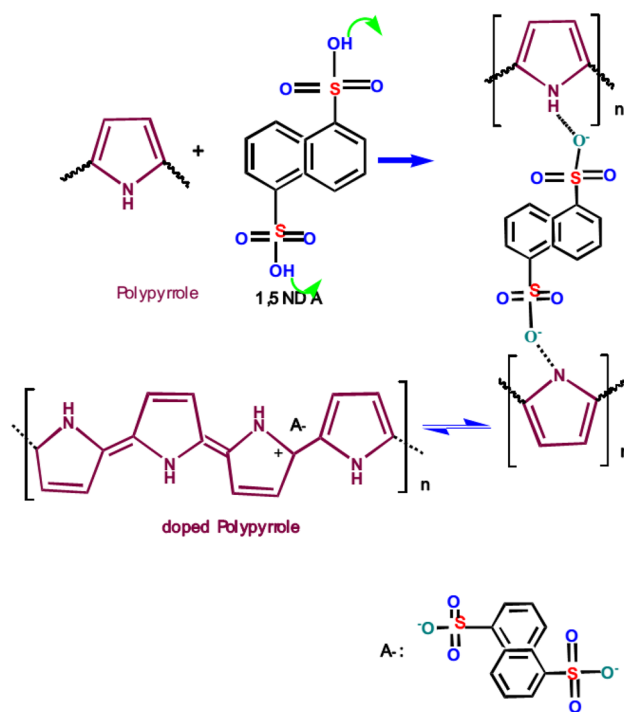
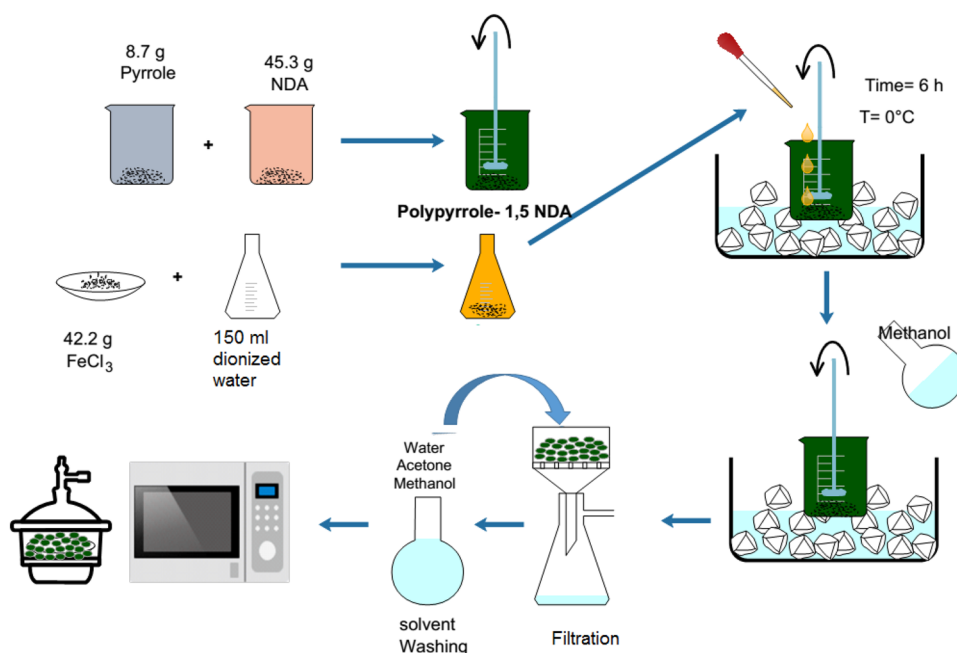
Phenol (99%) was purchased from Alpha Aesar (Germany). Aniline (99%) and paraformaldehyde (99%) were acquired from VWR Chemicals (France). The typical nonfunctional phenol A-aniline-based benzoxazine monomer was synthesized from phenol, aniline, and paraformaldehyde at a molar ratio of 1:2:4, according to the solventless technique that was reported by Ning and Ishida [27]. Dichloromethane, chloroform, sodium hydroxide, ammonium persulfate, hydrochloric acid, and tetrahydrofuran were obtained from Honeywell Riedel-de-Haen (Germany). Pyrrole (Sigma–Aldrich; 98%) was distilled under vacuum and stored in a refrigerator. Iron (III) chloride hexahydrate (FeCl₃·6H₂O) (analytical grade, Sigma–Aldrich) and 1,5-naphthalene disulfonic acid

(NDA) (97% purity, Sigma-Aldrich) were used without further purification.

2.2 Synthesis of 1,5-naphthalene disulfonic acid-doped polypyrrole nanoparticles (NDA.PPy)

The chemical polymerization of pyrrole was achieved using a one-step synthesis method as shown in Scheme 1. To begin, 8.7 g of freshly double-distilled pyrrole and 45.3 g of NDA were dissolved in 150 mL of deionized water while being vigorously magnetically agitated to ensure good dispersion and a homogeneous system. On the other hand, 42.2 g of FeCl_3 were dissolved in 150 mL of deionized water. The two solutions were cooled to 0 °C. At this temperature, the FeCl_3 solution was slowly dropped into the dispersed pyrrole and 5-naphthalene disulfonic acid (NDA) solution and stirred for 6 h. To stop the reaction, excessive quantity of methanol was added to the mixture. The precipitated polypyrrole was filtered under vacuum and washed several times with distilled water, ethanol, and acetone to eliminate the unreacted chemicals. Finally, the resultant black cake was dried in an oven at 60 °C overnight, milled into fine powder, and kept in a desiccator. The chemical reactions involved in the synthesis of 1,5-naphthalene disulfonic acid-doped polypyrrole nanoparticles and its chemical structure are graphically depicted in Scheme 2.

Scheme 1 Synthesis steps of 1,5-naphthalene disulfonic acid-doped polypyrrole nanoparticles



Scheme 2 The chemical reactions involved in the synthesis of 1,5-naphthalene disulfonic acid-doped polypyrrole nanoparticles

2.3 Preparation of polybenzoxazine/NDA.PPy nanocomposites

The polybenzoxazine/NDA.PPy nanocomposites

were produced by adding different weight ratios of NDA.PPy, in the range of 5–20 wt%, into 20 ml of dichloromethane containing 2 g of benzoxazine monomer (P-a). The resulting mixtures were then ultrasonically treated for 2 h to ensure homogeneous dispersion of NDA.PPy into the thermosetting matrix. The obtained solutions were then dried to evaporate the solvent and afford viscous black cakes, which were then poured into the respective molds and melted at 80 °C. The thermal curing process for the corresponding poly(P-a)/NDA.PPy was initiated using a graded thermal curing program of 120 °C, 160 °C, and 180 °C for 2 h.

2.4 Characterization

Fourier transform infrared (FTIR) spectra of the developed specimen were acquired using a PerkinElmer 100 spectrometer equipped with a deuterated triglycine sulfate (DTGS) detector and KBr optics. Transmission spectra were recorded from 4000 to 500 cm^{-1} with a resolution of 4 cm^{-1} after averaging two scans by casting a thin film on a KBr plate. Raman spectra of the synthesized NDA.PPy PPy conductive nanofillers were investigated using a Micro Raman System RM3000 spectrometer and an excitation laser wavelength of 532 nm, which was focused onto the specimen using a microscope with a X100 objective.

To evaluate the effect of PPy on the curing behavior of benzoxazine monomer, DSC experiments were carried out on a DSC 2920 model from TA Instruments with a heating rate of 20 °C/min and a nitrogen flow rate was recorded with 60 ml/min for all tests. The Zetasizer AT is a “Malvern Panalytical” instrument that uses light scattering to determine particle size in the range of 1 to 1000 nm with an accuracy of +/-2%. To determine the particle size of NDA.PPy nanoparticles, a solution of 0.5 wt% nanoparticles dispersed in water was used. To assess the dispersion state in poly(P-a)/NDA.PPy nanocomposite specimens, a scanning electron microscope (SEM) (FEI-Quanta 600) at voltages of 15 kV and 5 kV was used.

Direct current electrical conductivity (σ_{DC}) tests were performed at room temperature on the pure poly(P-a) matrix and its highly resistive nanocomposites filled with NDA.PPy ($< 10^{-7} \text{ S.cm}^{-1}$)

by a Keithley 6517 A electrometer connected to a Keithley 8009 test fixture following the 2-probe standard technique. On the other hand, the electrical conductivities of conductive poly(P-a)/NDA.PPy nanocomposites ($\sigma_{\text{DC}} > 10^{-7} \text{ S.cm}^{-1}$) were precisely obtained by means of the 4-probe standard technique using a Jandel RM3000 apparatus at room temperature. The dimensions used for the nanocomposite specimens in this test were a square form of $10 \times 10 \times 1 \text{ mm}^3$.

The Alternating current conductivity σ_{AC} of the prepared nanocomposite systems were determined with the help of an impedance analyzer (Solartron impedance/gain phase analyzer 1260) using a platinum (Pt) electrode at 21 °C at a frequency range of 100 Hz to 1 MHz. All specimens were completely dried before coating with conducting silver evenly and shaped to plates with a diameter around 20 mm. This experiment was repeated three times under the same conditions.

The EMI SE and dielectric properties of poly(P-a)/NDA.PPy nanocomposites were evaluated in the microwave frequency range of 8.2–12.4 GHz (X-band), using a standard rectangular waveguide and a 2-port Vector Network Analyzer (model 8719ES, Agilent Technologies, Santa Clara, California). The real part (dielectric constant, ϵ') and imaginary part (dielectric loss, ϵ'') of the permittivity of the tested nanocomposites were obtained by Agilent 85071 software. The EMI SE, which represents the amount of electromagnetic radiation attenuated in a specific material, can be thus measured. In the present study, EMI SE was calculated from the S_{12} (S_{21}) measurements (S-parameters) [3] using Eq. (1).

$$EMISE(dB) = 10\log_{10}\left(\frac{1}{|S_{12}|^2}\right) + 10\log_{10}\left(\frac{1}{|S_{21}|^2}\right), \quad (1)$$

where $|S_{12}|$ denotes the transmitted power from port 1 to port 2.

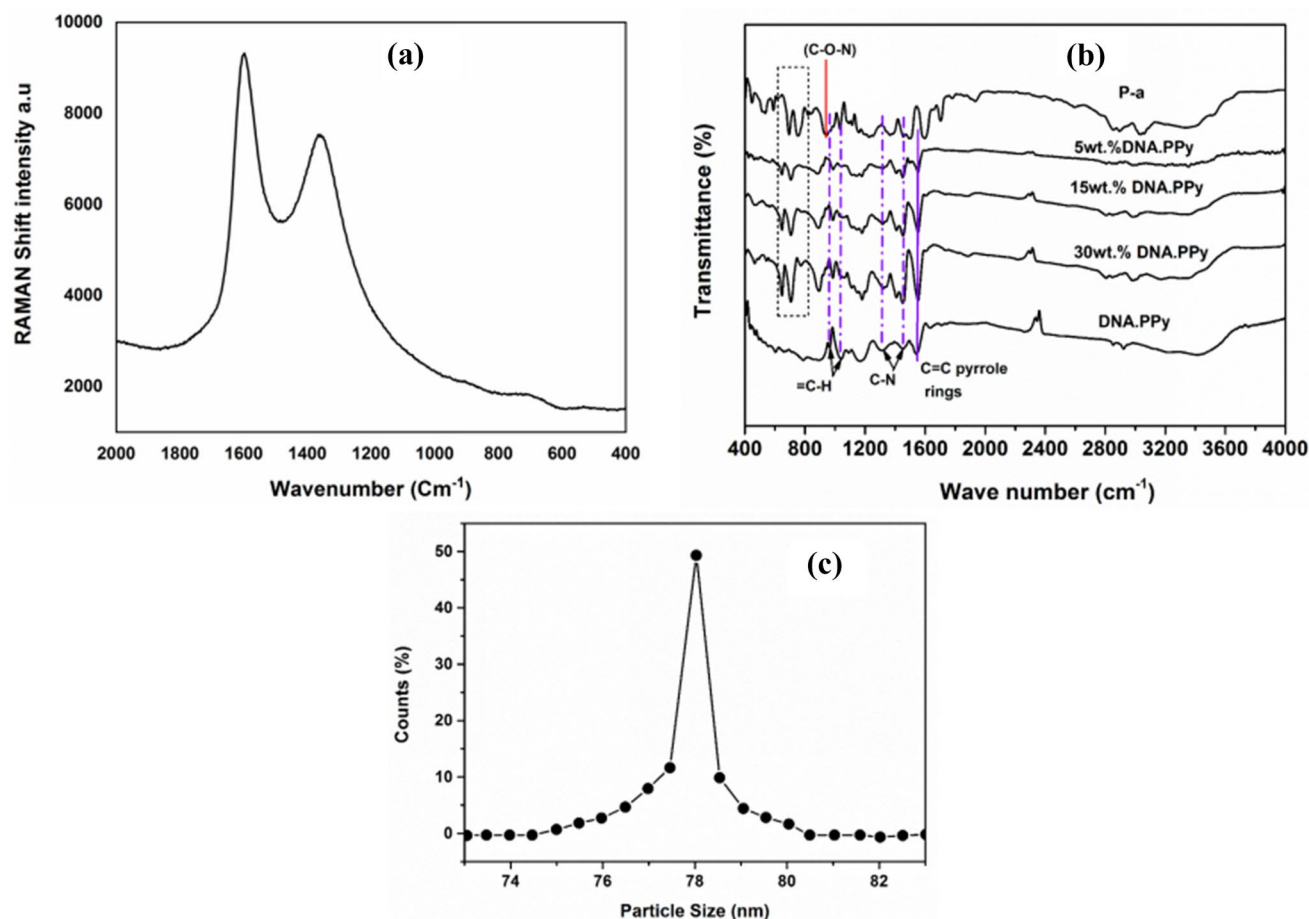


Fig. 1 **a** Raman spectra for the as-synthesized NDA.PPy nanoparticles and **b** FTIR spectra of P-a/NDA.PPy nanocomposites, and **c** Particle size distribution of NDA.PPy nanoparticles

3 Results and discussion

3.1 Structural analysis

To characterize the structural features of NDA.PPy nanofillers, Raman spectrum was carried out with an excitation laser wavelength of 532 nm. In Fig. 1A, a typical intense tangential resonance absorption band (G band) at 1559 cm^{-1} and a defect band (D band) at 1375 cm^{-1} were detected in the spectrum of the as-synthesized NDA.PPy, which correspond to the C=C backbone stretching and the ring stretching mode of PPy, respectively [28]. In our case, the intensity ratio of the D band to that of the G band (I_D/I_G) for the NDA.PPy reached 0.78, which is similar to the ratios reported in the literature [29].

The FTIR spectra of P-a monomer, DNA.PPy, and their resulting P-a/DNA.PPy mixtures containing 5, 15, and 30 wt% of DNA.PPy nanofillers are depicted

in Fig. 1B. The curve of P-a clearly showed the existence of the all well-known characteristic peaks of benzoxazine structure, for example, the peak at 944 cm^{-1} is related to the characteristic mode of benzene with an attached oxazine ring [21]. The bands at 1228 and 1075 cm^{-1} are ascribed to the asymmetric and symmetric stretching of C-O-C, respectively. The CH_2 wagging and asymmetric stretching modes of C-N-C are detected at 1323 and 1158 cm^{-1} , respectively [18]. Likewise, the band at 1497 cm^{-1} is attributed to the trisubstituted benzene ring. On the other hand, the FTIR spectrum of NDA.PPy revealed the presence of methyl and methylene group absorption bands at 2965 , 2931 , 2894 , and 2866 cm^{-1} , respectively [28]. Also, the absorption bands related to the in plane deformation and stretching vibrations of C-N bond occur at 1457 cm^{-1} and 1290 cm^{-1} , respectively. The appearance of peaks at 1044 and 914 cm^{-1} related to the vibration of polypyrrole =C-H groups are also identified [27].

Furthermore, the band related to the vibration of the C=C bond of the pyrrole rings appears at 1543 cm^{-1} . From the FTIR spectra of P-a/DNA.PPy nanocomposites, it appears clearly that the absorption bands of both components for example, the intensity of the band corresponding to the vibration of the C=C bond of the pyrrole at 1543 cm^{-1} is increased as the DNA.PPy loading in the mixtures increased. These results confirm the successful synthesis of the P-a monomer, DNA.PPy, and their nanocomposites.

The particle size of NDA.PPy nanoparticles was determined by means of "ZetaSizer AT" using a 0.5 wt% solution of nanoparticles dispersed in pure water. Figure 1C illustrates the resulting particle size distribution. The average particle size for the synthesized NDA.PPy is 78 nm.

The morphology of the prepared NDA.PPy was observed by TEM and SEM, while the neat poly(P-a) and their resulted nanocomposites filled with 10 wt%, 20 wt%, and 30 wt% were examined using SEM and the corresponding collected images are depicted in Fig. 2. The morphology of PPy appeared in the form of granules, as shown from the TEM and SEM photos in Fig. 2a, b, respectively [30]. However, the cured polybenzoxazine resin shows a smooth, textured,

contour less structure, as depicted in Fig. 2(c) [31]. Further micrographs of PPy-loaded poly(P-a) matrix in Fig. 2d–f revealed significant changes in the morphology of polybenzoxazine matrix, which transformed from glassy structure to a rough and irregular form, which means that the ring-opening polymerization of P-a rings were started on the granular surface of the interconnected linear network of PPy. Thus, the addition of PPy resulted in interlocked layers covered with the benzoxazine matrix over the surface. This interlayered morphology is generated due to hydrogen bonding and π - π stacking interaction between NDA.PPy with benzene rings of poly(P-a) which promote the compatibility in these nanocomposites [32]. On the other hand, the addition of NDA.PPy fillers are straightforwardly dispersed into the polybenzoxazine matrix and form adjacent connecting patterns, which play the role of conductive paths.

3.2 Curing behavior

The curing behavior of P-a monomer and its resulting nanocomposites were evaluated by means of DSC in the temperature range of $40\text{ }^{\circ}\text{C}$ to $350\text{ }^{\circ}\text{C}$. The recorded thermograms of nanocomposites are displayed in

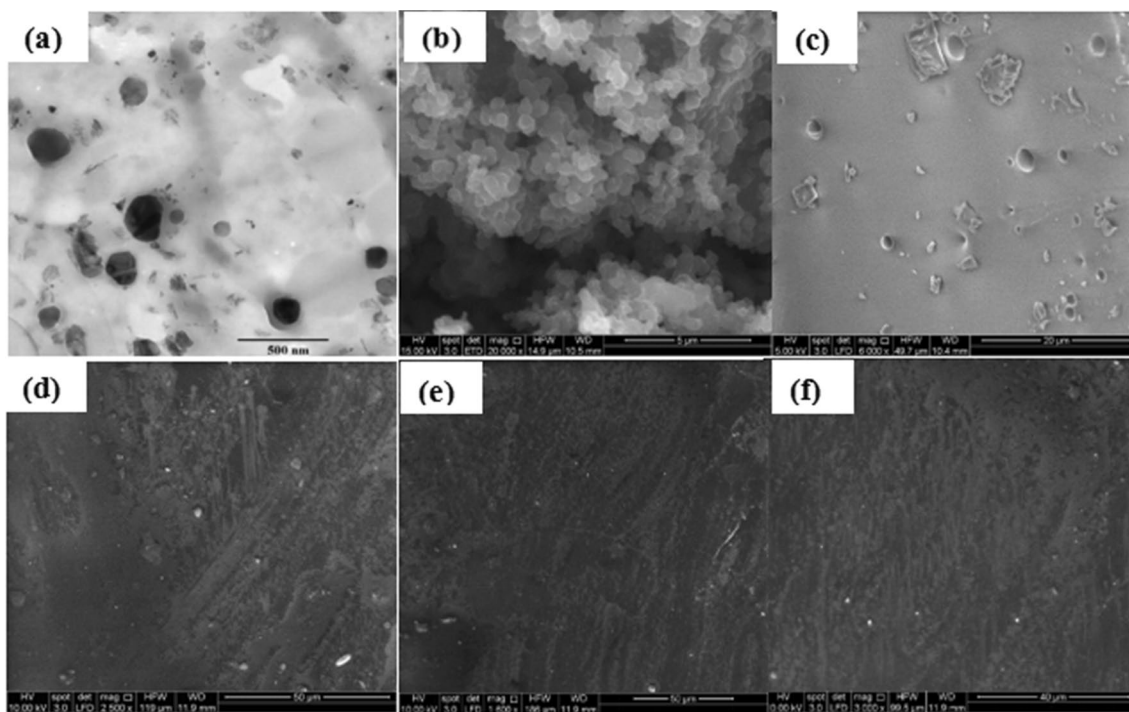


Fig. 2 a TEM image as-synthesized NDA.PPy and b SEM images of NDA.PPy, c SEM images of poly(P-a), d–f SEM images of poly(P-a)/NDA.PPy nanocomposite containing 10 wt%, 20 wt%, and 30 wt% of NDA.PPy nanofillers, respectively

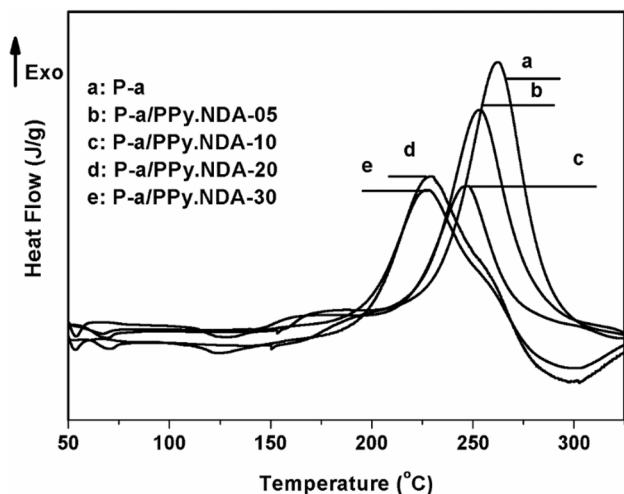
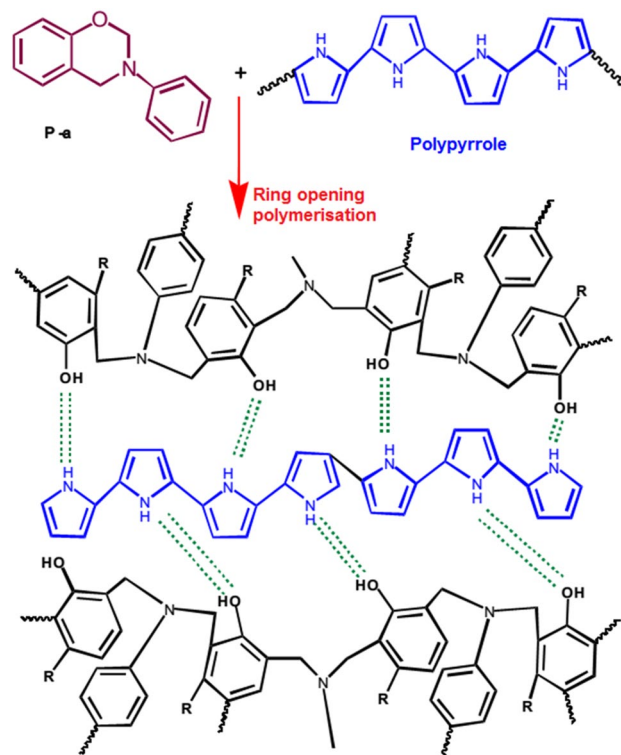


Fig. 3 DSC curves of uncured P-a/NDA.PPy nanocomposite mixtures

Table 1 Curing characteristics of P-a monomers with different wt% of NDA.PPy.

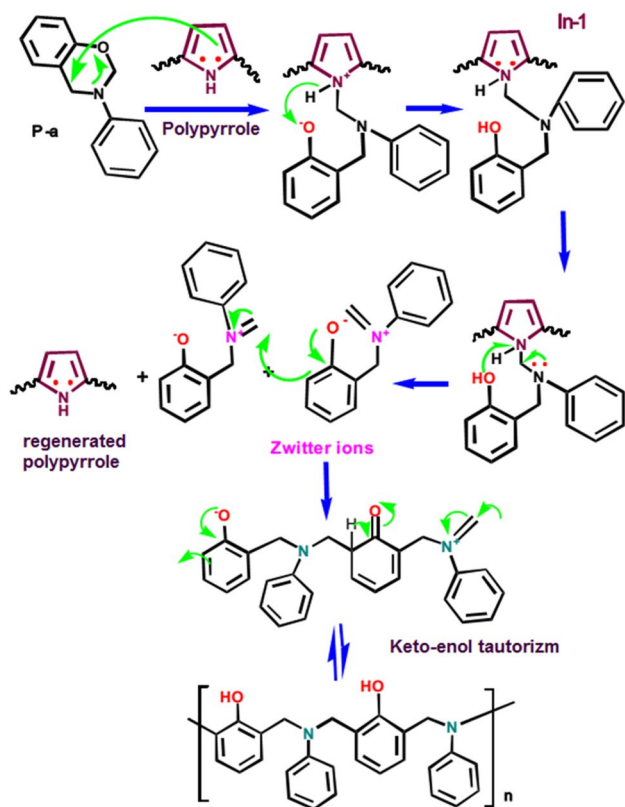
| NDA.PPy (Wt.%) | Onset Temperature (°C) | Peak Temperature (T_p) (°C) | ΔH (J/g) |
|----------------|------------------------|---------------------------------|------------------|
| 0 | 221.2 | 261.4 | 356 |
| 5 | 209.6 | 253.1 | 311.5 |
| 10 | 205.3 | 247.3 | 256.3 |
| 20 | 177.2 | 230.5 | 233.8 |
| 30 | 173.4 | 224.7 | 208.6 |

Fig. 3 and the curing data are collected in Table 1. The exothermic curing onset of P-a monomer, due to the ring-opening polymerization, starts at 221.2 °C and finalizes at 261.4 °C. Accordingly, the trisubstituted benzene ring transforms into a tetrasubstituted rings and a three-dimensional polybenzoxazine is formed as illustrated in Scheme 3. Aiming to reduce this temperature, the curing process of P-a monomer is investigated in the presence of various ratios of nitrogen-rich, conductive NDA.PPy. The addition of NDA.PPy conductive nanofillers gradually reduced the curing temperature of the P-a monomer, as expected. In addition, the appearance of a single exothermic peak for the P-a/NDA.PPy nanocomposites indicates that polymerization occurs in a single step. The inclusion of 30 wt% of NDA.PPy resulted in a decrease in the curing peak temperature of 36.7 °C. In addition, a remarkable decrease in the onset of curing temperatures and enthalpy of cure (ΔH) of these nanocomposites are equally detected as shown in Table 1. This



Scheme 3 The curing process of P-a benzoxazine monomer in the presence of NDA.PPy nanoparticles

results are attributed to the great capacity of NDA.PPy to decrease the exothermic nature of curing process through the construction of low energy activation path due to its acidic characteristics. In addition, like other types of amides and oligomeric amines, which has a secondary amine on five membered hetero rings, NDA.PPy is also considered as very effective modifier to heatless catalyze the ring-opening process of benzoxazine resins, which is in accordance with several reported studied [33]. In the presence of polypyrrole, a decrease in the curing temperature of the benzoxazines was observed, which can be attributed to the catalytic nature of polypyrrole. When the nitrogen atom of the polypyrrole ring with its lone pair is heated, it initiates the ring opening of benzoxazine moieties, leading to the formation of Intermediate-I (In-1). Intermediate-I can further proceed through two pathways. In the first pathway, the lone pair on the tertiary nitrogen undergoes a highly feasible migration, followed by a prototropic shift, resulting in the formation of a Zwitterion (consisting of an iminium nitrogen cation and a secondary carbanion) and the regeneration of polypyrrole. The secondary carbanion of the Zwitterion then attacks the iminium nitrogen



Scheme 4 Mechanism of PPy-assisted curing reaction of P-a benzoxazine monomer

cation of another Zwitterion in a chain reaction, followed by keto-enol tautomerism, ultimately resulting in the formation of the polybenzoxazine network with polypyrrole stacking in between. On the other hand, the second process involving the less feasible migration of the lone pair on the nitrogen atom of the pyrrole moiety only leads to the formation of an unstable methylene pyrrolium cation. Therefore, the first mechanism adequately explains the catalytic activity of the regenerated polypyrrole, as shown in Scheme 4. Additionally, it is expected that the linear and amorphous nature of PPy promotes interaction with benzoxazine monomers. Consequently, the addition of 5 wt% to 30 wt% NDA.PPy to the benzoxazine monomer P-a results in a significant reduction in the curing temperature and curing enthalpy of the mixed P-a/NDA.PPy systems. Based on these findings, it can be concluded that NDA.PPy exhibits catalytic activity similar to other amines [33–35].

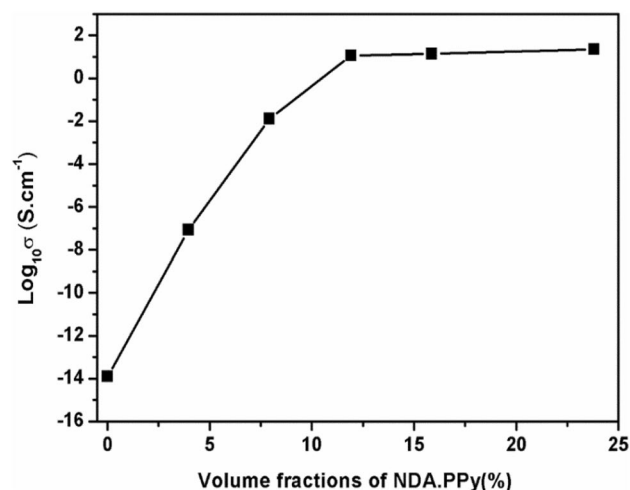


Fig. 4 The DC electrical conductivity of poly(P-a)/NDA.PPy nanocomposites at various nanofiller ratios

3.3 Electrical conductivity

3.3.1 DC electrical conductivity

The evolution of electrical conductivity (σ) of poly(P-a)/NDA.PPy nanocomposites at various nanofiller ratios are depicted in Fig. 4. The pure poly(P-a) demonstrated an isolated feature with a very small electrical conductivity value of $1.24 \times 10^{-14} \text{ S.cm}^{-1}$. However, the electrical conductivity of the developed poly(P-a)/NDA.PPy nanocomposites are enhanced by increasing the NDA.PPy ratio to reach its maximum value of 22.3 S.cm^{-1} at 30 wt%, due to the construction of conducting paths into the polybenzoxazine matrix, as previously found from their morphological analysis microstructures. Also, a sharp increase in the electrical conductivity of these nanocomposites (approximately eleven orders of

Table 2 The electrical properties of poly(P-a)/PPy.NDA nanocomposites

| NDA.PPy (wt%) | NDA.PPy (vol%) | σ (S.cm ⁻¹) | Log ₁₀ (σ) (S.cm ⁻¹) |
|---------------|----------------|--------------------------------|--|
| 0 | 0 | 1.24×10^{-14} | -13.91 |
| 5 | 3.97 | 8.45×10^{-8} | -7.07 |
| 10 | 7.93 | 1.3×10^{-2} | -1.89 |
| 15 | 11.92 | 11.4 | 1.06 |
| 20 | 15.87 | 13.8 | 1.14 |
| 30 | 23.81 | 22.3 | 1.35 |

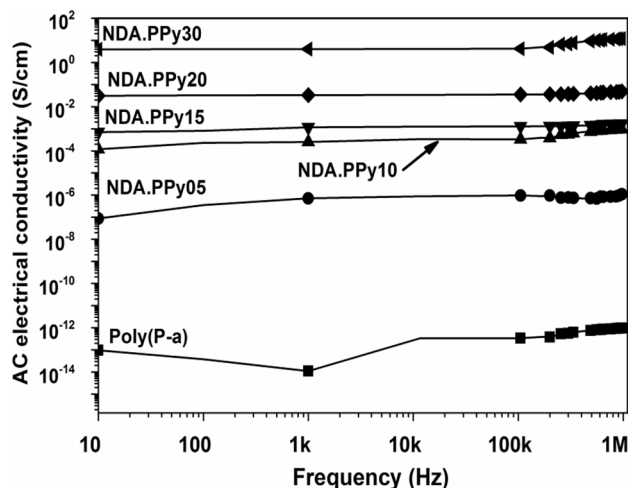


Fig. 5 Frequency-dependent AC electrical conductivity of poly(P-a)/NDA.PPy nanocomposites

magnitude) is noted between 5 wt% (3.97 vol%) and 15 wt% (11.92 vol%) NDA.PPy content, reflecting that the percolation threshold of these nanocomposites is around 10 wt%. This clearly indicates an insulator–conductor transition as the NDA.PPy nanoparticles construct a conductive network within the poly(P-a) matrix. Expectedly, the increase in electrical conductivity for these nanocomposites was more pronounced after the percolation threshold (10 wt%), which can be justified by the higher aspect ratio and the improved dispersion state of NDA.PPy filler into polybenzoxazine matrix (Table 2) [36].

3.3.2 AC electrical conductivity

Figure 5 illustrates the results of frequency-dependent AC electrical conductivity measurements conducted on poly(P-a)/NDA.PPy nanocomposites at room temperature. The neat poly(P-a)-based thermoset behaves as an electrical insulator with a conductivity of approximately 10^{-13} S/cm. However, the addition of a mere 5 wt% of NDA.PPy significantly enhances the electrical conductivity of the nanocomposite to 5×10^{-7} S/cm at 10 Hz. As the frequency increases from 10 Hz to 1 MHz, the electrical conductivity values further increase to 9.88×10^{-4} , 17×10^{-3} , and 4.96×10^{-2} for poly(P-a)/NDA.PPy nanocomposites containing 10 wt%, 15 wt%, and 20 wt% NDA.PPy, respectively. The highest electrical conductivity of 12.3 S/cm is observed in the nanocomposite containing 30 wt% of NDA.PPy. The frequency-independent plateau region indicates

the formation of a percolating network-like structure of NDA.PPy within the poly(P-a) nanocomposite. This suggests that the constant conductivity represents the direct current conductivity, which increases with the higher weight fractions of NDA.PPy in the nanocomposites. Consequently, an increase in the NDA.PPy content leads to enhanced electrical conductivities in polybenzoxazine nanocomposites due to the development of conducting paths within the matrix [37, 38]. The significant change in conductivity with respect to filler content can be attributed to the dispersion mode of the filler. At lower filler contents (< 5 wt%), the filler particles, in various shapes and sizes, are uniformly distributed within the insulating matrix, with larger distances between adjacent filler particles. However, as the filler content increases, the interfacial interaction between the individual filler particles and the polymeric matrix improves, increasing the probability of developing a conductive network throughout the matrix. This phenomenon highlights the homogeneous dispersion of NDA.PPy nanofillers in the polybenzoxazine matrix and their inherent higher electrical conductivity.

3.4 Electromagnetic shielding properties

Total EMI SE is defined as the sum of three main EMI attenuation mechanisms: reflection loss (SE_R), absorption loss (SE_A), and multiple internal reflection loss at the material interface (SE_M) (conductive fillers or porosity). In the present study, the multiple reflection effects were neglected as they cannot be evaluated as a distinct factor [39]. The transmittance (T) and reflectance (R) coefficients were determined through the S-parameters obtained by the vector network analyzer [40, 41], as given in Eqs. (2) and (3):

$$T = \left| \frac{E_T}{E_i} \right| = |S_{12}|^2 = |S_{21}|^2 \tag{2}$$

$$R = \left| \frac{E_R}{E_i} \right| = |S_{11}|^2 = |S_{22}|^2. \tag{3}$$

The absorbed coefficient was computed, by taking into account that the incident power utilized in the measurements was 5 dB, using Eq. (4).

$$A = I - T - R. \tag{4}$$

The total EMI SE average, absorption loss (SE_A), and reflection loss (SE_R) were determined from the

transmittance (T) and reflectance (R) coefficients and assessed by using Eqs. (5, 6, 7) [40].

$$\begin{aligned} EMI\ SE &= SE_R + SE_A = 10\log\left(\frac{I}{I-R}\right) + 10\log\left(\frac{I-R}{T}\right) \\ &= 10\log\left(\frac{I}{T}\right) \end{aligned} \quad (5)$$

$$SE_R = 10\log\left(\frac{I}{I-R}\right) \quad (6)$$

$$SE_A = 10\log\left(\frac{I-R}{T}\right) \quad (7)$$

when an EM wave hits a polybenzoxazine/NDA.PPy nanocomposite shield, the electrons and other charged particles inside this shield respond to the incident wave by creating a scattered field or induced field. The induced field changes the total field inside the shield, which affects the charge motion. Three different mechanisms contribute to the shielding of an incident EM wave, namely reflection R , absorption A , transmission T , and multiple reflection MR [42]. The addition of conductive polypyrrole nanoparticles to a poly(P-a) matrix can lead to changes in the absorption, reflection, and transmission coefficients of their resulted nanocomposite material. These effects are mainly driven by the unique electrical and electromagnetic properties of PPy nanofillers, such as their strong absorption characteristics, electrical conductivity modifications, and EM-scattering performance. The concentration, dispersion, and size of PPy nanoparticles

within the polybenzoxazine matrix can control the final EM shielding properties of their composites [43].

3.4.1 Effect of NDA.PPy loadings on the EMI SE of nanocomposites

The influence of NDA.PPy conductive filler content on the average total EMI SE, which comprises the absorption phenomena, reflection phenomena, and the electrical conductivity of the studied nanocomposites, is shown in Fig. 6. The EMI SE tests were carried out in the X-band frequency range (8.2 at 12.4 GHz) on nanocomposite specimens with a thickness of 2 mm. It is observed that the pure poly(P-a) has the lowest EMI SE value of 1.1 dB. In addition, lower values are detected for nanocomposites filled with NDA.PPy filler before their percolation thresholds, which corresponds to 10 wt%. However, after the percolation threshold, the developed nanocomposites demonstrated dissimilar behaviors due to the formation of conductive networks, where the EMI SE values are significantly increased to reach their maximum value of 27.2 at 30 wt% NDA.PPy loading. These nanocomposite shields tend to be conductive, due to mobile charge carriers as confirmed by previous research works [44]. Our newly explored nanocomposites showed higher EMI SE values compared to some polyurethane and epoxy systems containing NDA.PPy conductive fillers, as reported in the literature [45–47].

Table 3 lists the experimental data on the total EMI SE average, SE_A , SE_R , and the EMI SE percentage by absorption for the studied nanocomposites. In the case of poly(P-a)/NDA.PPy nanocomposites with higher nanofiller content, SE_A rises and SE_R becomes fixed. This behavior is attributed to the high dielectric

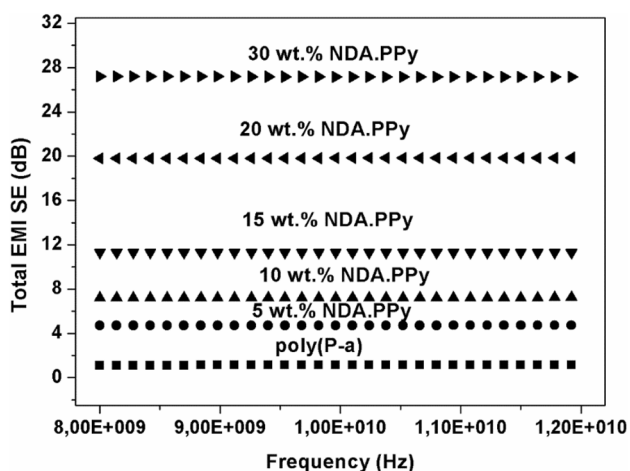


Fig. 6 The variation of total EMI SE values of poly(P-a)/NDA.PPy with frequency at X-band

Table 3 Total EMI SE average, SE_A , SE_R , and percentage of EMI SE by absorption of the developed nanocomposites having a thickness of 2 mm

| NDA.PPy (wt%) | Total EMI SE_T (dB) | SE_A (dB) | SE_R (dB) | SE_A (%) |
|---------------|-----------------------|-------------|-------------|------------|
| 0 | 1.1 ± 0.1 | 0.1 ± 0.1 | 0.8 ± 0.1 | 9 |
| 5 | 4.7 ± 0.2 | 1.1 ± 0.2 | 3.6 ± 0.2 | 23 |
| 10 | 7.2 ± 0.3 | 4.1 ± 0.1 | 3.1 ± 0.6 | 57 |
| 15 | 11.3 ± 0.2 | 7.1 ± 0.3 | 4.2 ± 0.2 | 63 |
| 20 | 19.8 ± 0.6 | 15.1 ± 0.6 | 4.7 ± 0.1 | 76 |
| 30 | 27.2 ± 0.1 | 21.9 ± 0.1 | 5.3 ± 0.2 | 81 |

loss of NDA.PPy nanofiller-reinforced polybenzoxazine nanocomposites and reflects a trend between the absorption mechanism and nanofiller ratio. In addition, exceeding the percolation threshold makes SE_A as the principal EMI shielding mechanism for both (2 and 5 mm) nanocomposites. This is ascribed to the formation of conductive routes in the polybenzoxazine matrix, which eases the charge carrier movement, increases electromagnetic radiation contacts, and the existence of electric and/or magnetic dipoles in the polybenzoxazine/NDA.PPy shielding material, which interacts with the electromagnetic field. Therefore, high EMI SE and SE_A values were detected for the poly(P-a)/NDA.PPy nanocomposites as the conductive NDA.PPy nanofiller content increased while the SE_R values remained practically unchanged. These effects, however, were not observed in pure poly(P-a) or its

nanocomposites, which have lower electrical conductivity values (lower than $8.45 \times 10^{-8} \text{ S.cm}^{-1}$).

3.4.2 Effect of nanocomposite thickness on the total EMI SE

The effect of poly(P-a)/NDA.PPy specimen thickness (2 and 5 mm) on the total EMI SE was studied, and the measured EMI SE, SE_A , SE_R , and the percentage of EMI SE by absorption data of the nanocomposite with 5 mm thickness are summarized in Table 4. As anticipated, the EMI SE values of specimens having a thickness of 5 mm are more pronounced than those with a 2 mm thickness. This result is probably due to the increased shielding efficiency by absorption mechanism in the thick nanocomposites, as the shielding efficiency by reflection mechanism (SE_R) value was almost fixed [48]. The 5-mm-thick nanocomposite containing 30 wt% of NDA.PPy demonstrated an EMI SE of approximately 46.4 dB, which is more than one and a half times recorded for a similar nanocomposite with 2 mm thickness (27.2 dB).

Table 4 Total EMI SE_T average, SE_A , SE_R , and percentage of EMI SE by absorption of some poly(P-a)/NDA.PPy nanocomposites having a thickness of 5 mm

| PPy content (wt%) | Total EMI SE, dB | SE_A , dB | SE_R , dB | EMI SE_A , % |
|-------------------|------------------|----------------|---------------|----------------|
| 10 | 18.1 ± 0.5 | 12.2 ± 0.1 | 5.9 ± 0.3 | 67 |
| 20 | 25.6 ± 0.3 | 19.5 ± 0.3 | 6.1 ± 0.2 | 76 |
| 30 | 46.4 ± 0.1 | 40.1 ± 0.4 | 6.3 ± 0.2 | 86 |

3.5 Dielectric properties of nanocomposites

The complex permittivity ($\epsilon^* = \epsilon' - j\epsilon''$) of poly(P-a)/NDA.PPy nanocomposites were determined directly from scattering parameters and phase shift measurements by following the standard Nicholson–Ross–Weir

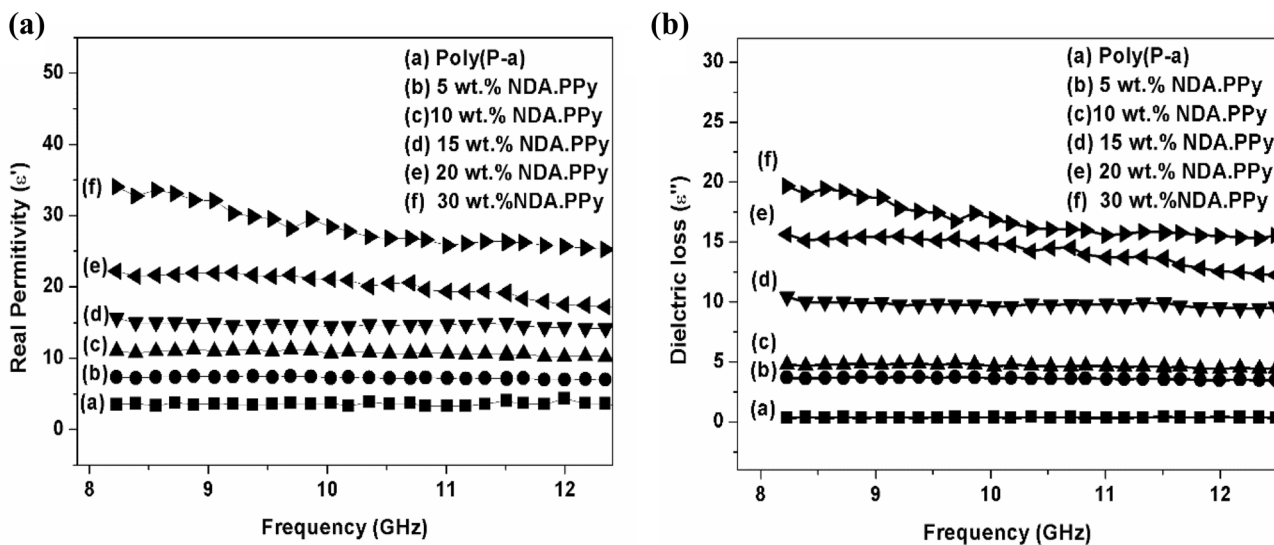


Fig. 7 Variation of **a** Real and **b** imaginary part of permittivity of poly(P-a)/NDA.PPy at various weight ratios nanocomposites with X-band frequencies

technique [49]. The real (ϵ') and imaginary (ϵ'') permittivity of the poly(P-a) matrix and their resulting 2 mm-nanocomposites as a function of frequency in the X-band are shown in Fig. 7. Both ϵ' and ϵ'' are enhanced with the rising of PPy.NDA content due to the formation of conductive chains, which provokes higher dipole intensity and improves the interfacial polarization phenomena. Expectedly, the values of ϵ' and ϵ'' of poly(P-a)/NDA.PPy nanocomposites are higher than that of the unfilled resin due to the homogeneous dispersion of conductive NDA.PPy nanofillers into this matrix, which increases the dipole intensities and promotes the interface polarization, which increases the shielding efficiency values by absorption mechanism (SE_A). Furthermore, minor resonant effects and fluctuations for ϵ' and ϵ'' are detected with increasing frequency beyond the percolation threshold for the poly(P-a)/NDA-PPy nanocomposites. These effects are most commonly observed in polymer composites filled with conductive high aspect ratio nanofiller and exhibiting increased electrical conductivity [50].

4 Conclusions

Electrically conductive polybenzoxazine nanocomposites filled with NDA.PPy conductive fillers were successfully produced with a thickness of 2 and 5 mm and their curing behavior, electrical, and shielding properties were evaluated. DSC analysis confirmed the heatless catalytic effect of doped polypyrrole, where a significant reduction in the curing temperature and the enthalpy of cure as the contents of NDA.PPy are increased. As the ratio of nanofillers increased in the polybenzoxazine matrix, the EMI SE, the AC electrical conductivity, and the DC electrical conductivity were gradually increased; this was due to the high aspect ratio of the fillers used, which eased the construction of well-dispersed conducting pathways even at lower amounts of filler (percolation threshold of 10 wt% NDA.PPy). In addition, the concentration of conductive fillers influenced the electromagnetic interference attenuation mechanism; as the NDA.PPy loading into the thermosetting matrix increased, so did the absorption loss (SE_A). Moreover, the EMI SE data of these nanocomposites were affected by both their

thicknesses and their tested frequencies. Furthermore, as the PPy.NDA ratio increased in the matrix, both the dielectric constant and dielectric loss values for the newly developed nanocomposites were significantly increased, which reflects the presence of higher dipolar and interfacial polarization. Remarkably, the addition of conductive NDA.PPy nanofillers into the polybenzoxazine thermoset enhanced its shielding efficiency by absorption loss mechanism, where a total EMI SE of 27.2 (81% by absorption loss) and 46.4 dB (86% by absorption loss) were recorded for the 2- and 5-mm-thick nanocomposites containing 30 wt% NDA.PPy, respectively. These findings indicate that the newly developed polybenzoxazine/NDA.PPy nanocomposites can meet the requirements of many industrial electromagnetic radiofrequency shielding applications by shielding more than 99.9% of incident radiation in the X-band.

Author contributions

NR: conceptualization; investigation; methodology; writing original draft. E-OM: project administration; resources; supervision; validation. MSR: resources; validation; review and editing. MM: investigation; validation; review and editing. HM: investigation; validation; review and editing. NA: resources; review and editing. MD: resources; review and editing.

Funding

The authors have not disclosed any funding.

Data availability

The datasets generated during and/or analyzed during the current study are available from the corresponding author on reasonable request.

Declarations

Conflict of interest The authors report no conflict of interest.

References

1. T. Wu, T.S. Rappaport, C.M. Collins, *IEEE Micro. Mag.* **16**, 65–84 (2015). <https://doi.org/10.1109/MMM.2014.2377587>
2. V. Zaroushani, A. Khavanin, A. Jonidi Jafari, S.B. Mortazavi, F. Khajenasiri, *J. Health Saf. Work.* **6**, 1–16 (2016)
3. S. Geetha, K.K. Satheesh Kumar, C.R.K. Rao, M. Vijayan, D.C. Trivedi, *J. Appl. Polym. Sci.* **112**, 2073–2086 (2009). <https://doi.org/10.1002/app.29812>
4. L. Zhong, R. Yu, X. Hong, *Text. Res. J.* **91**, 1167–1183 (2021). <https://doi.org/10.1177/0040517520968282>
5. X. Wu, B. Wen, *Comp. Sci. Technol.* (2020). <https://doi.org/10.1016/j.compscitech.2020.108343>
6. V. Uma Varun, B. Rajesh Kumar, K.C. Etika, *Mater. Today: Proceed.* (2020). <https://doi.org/10.1016/j.matpr.2019.12.300>
7. M. Khodadadi Yazdi, B. Noorbakhsh, B. Nazari, Z. Ranjbar, *Prog Org. Coat.* **145**, 105674 (2020). <https://doi.org/10.1016/j.porgcoat.2020.105674>
8. H. Liu, Z. Huang, T. Chen, X. Su, Y. Liu, R. Fu, *Chem. Eng. J.* **427**, 131540 (2022). <https://doi.org/10.1016/j.cej.2021.131540>
9. L.L. Vovchenko, O.V. Lozitsky, L.Y. Matzui, V.V. Zagorodnii, *Appl. Nanosci.* **12**, 1037–1049 (2022). <https://doi.org/10.1007/s13204-021-01765-z>
10. M. González, J. Baselga, J. Pozuelo, *Carbon* (2019). <https://doi.org/10.1016/j.carbon.2019.02.068>
11. M.H. Al-Saleh, U. Sundararaj, *Carbon.* **47**, 1738–1746 (2009). <https://doi.org/10.1016/j.carbon.2009.02.030>
12. Y. Wang, X. Jing, *Polym. Adv. Technol.* **16**, 344–351 (2005)
13. N.E. Kamchi, B. Belaabed, J.-L. Wojkiewicz, S. Lamouri, T. Lasri, *J. Appl. Polym. Sci.* **127**, 4426–4432 (2012). <https://doi.org/10.1002/app.38036>
14. J.A. Pomposo, J. Rodríguez, H. Grande, *Synth. Met.* **104**, 107–111 (1999)
15. T. Mäkelä, S. Pienimaa, T. Taka, S. Jussila, H. Isotalo, *Synth. Met.* **85**, 1335–1336 (1997). [https://doi.org/10.1016/S0379-6779\(97\)80259-7](https://doi.org/10.1016/S0379-6779(97)80259-7)
16. A. Kaynak, J. Unsworth, R. Clout, A.S. Mohan, G.E. Beard, *J. Appl. Polym. Sci.* **54**, 269–278 (1994). <https://doi.org/10.1002/app.1994.070540301>
17. S. Sankaran, K. Deshmukh, M. Basheer Ahmed, S.K. Khadheer Pasha, *Comp. Part. A* **114**, 49–71 (2018). <https://doi.org/10.1016/j.compositesa.2018.08.006>
18. H.J. Kim, Z. Brunovska, H. Ishida, *Polymer* **40**, 1815–1822 (1999). [https://doi.org/10.1016/S0032-3861\(98\)00393-0](https://doi.org/10.1016/S0032-3861(98)00393-0)
19. Y.C. Su, F.C. Chang, *Polymer* **44**, 7989–7996 (2003). <https://doi.org/10.1016/j.polymer.2003.10.026>
20. H. Ishida, D.J. Allen, *J. Polym. Sci. Part. B* **34**, 1019–1030 (1996).
21. V.C. Kishore, R. Dhanya, K. Sreekumar, R. Joseph, K.C. Sudha, *Synth. Met.* **158**, 676–680 (2008). <https://doi.org/10.1016/j.synthmet.2008.04.012>
22. B. Kiskan, N.N. Ghosh, Y. Yagci, *Polym. Int.* **60**, 167–177 (2011). <https://doi.org/10.1002/pi.2961>
23. R. Chen, Q. He, X. Li, F. Wen, L. Cheng, L. Li, Y. He, X. Liu, J. Mu, *Chem. Eng. J.* **431**, 134049 (2022). <https://doi.org/10.1016/j.cej.2021.134049>
24. S. Zhang, T. Lan, D. Ren, X. Liu, Q. Ran, *J. Mater. Sci.* **56**, 10691–10705 (2021). <https://doi.org/10.1007/s10853-021-05977-0>
25. S. Zhang, S. Yin, Q. Ran, Q. Fu, Y. Gu, *Polym.* **162**, 20–28 (2019). <https://doi.org/10.1016/j.polymer.2018.12.024>
26. S. Zhang, Y. Wang, Q. Ran, Q. Fu, Y. Gu, *React. Funct. Polym.* **143**, 104324 (2019). <https://doi.org/10.1016/j.reactfunctpolym.2019.104324>
27. X. Ning, H. Ishida, *J. Polym. Sci. Part. A* **32**, 1121–1129 (1994). <https://doi.org/10.1002/pola.1994.080320614>
28. F. Gong, X. Xu, G. Zhou, Z.S. Wang, *Phys. Chem. Chem. Phys.* **15**, 546–552 (2013). <https://doi.org/10.1039/C2CP42790G>
29. Y. Wang, A.J. Wang, P.Y. Yang, W.X. Hu, X.N. Guo, J. Zhang, C. Li, C. Zhang, *J. Mater. Sci. Chem. Eng.* **5**, 26–43 (2017). <https://doi.org/10.4236/msce.2017.510003>
30. S.T. Navale, A.T. Mane, M.A. Chougule, R.D. Sakhare, S.R. Nalage, V.B. Patil, *Synth. Met.* **189**, 94–99 (2014). <https://doi.org/10.1016/J.SYNTHMET.2014.01.002>
31. K. Zhang, X. Tan, Y. Wang, H. Ishida, *Polym. (Guildf).* **168**, 8–15 (2019). <https://doi.org/10.1016/j.polymer.2019.01.089>
32. P. Pattanayak, N. Pramanik, P. Kumar, P.P. Kundu, *Int. J. Hydrog. Energ.* **43**, 11505–11519 (2018). <https://doi.org/10.1016/J.IJHYDENE.2017.04.300>
33. J. Sun, W. Wei, Y. Xu, J. Qu, X.D. Liu, T. Endo, *RSC Adv.* **5**, 19048–19057 (2015). <https://doi.org/10.1039/c4ra16582a>
34. J. Wang, Y.Z. Xu, Y.F. Fu, X.D. Liu, *Sci. Rep.* **6**, 1–7 (2016). <https://doi.org/10.1038/srep38584>
35. J. Zong, Q. Ran, *Chem. Select.* **4**, 6687–6696 (2019). <https://doi.org/10.1002/slct.201901447>
36. M.F. Shakir, I. Abdul Rashid, A. Tariq, A. Tariq, Y. Naw, A. Afzal, M. Nabeel, A. Naseem, U. Hamid, *J. Electron. Mater.* **49**, 1660–1665 (2020). <https://doi.org/10.1007/s11664-019-07631-7>
37. U. Cano-Castillo, L. Rejon, *J. New. Mat. Electrochem. Syst.* **4**, 37–40 (2001)

38. K. Nath, S.K. Ghosh, A. Katheria, P. Das, S.N. Chowdhury, P. Hazra, S. Azam, N.C. Das, *Polym. Adv. Technol.* **34**(3), 1019–1034 (2023). <https://doi.org/10.1002/pat.5949>
39. A. Gupta, V. Choudhary, *J. Mater. Sci.* **46**, 6416–6423 (2011). <https://doi.org/10.1007/s10853-011-5591-8>
40. M.F. Shakir, A. Tariq, Z.A. Rehan, Y. Nawab, I.A. Rashid, A. Afzal, U. Hamid, F. Raza, K. Zubair, M.S. Rizwan, S. Riaz, A. Sultan, M. Muttaqi, *SN Appl. Sci.* **2**, 706 (2020). <https://doi.org/10.1007/s42452-020-2535-4>
41. K. Zubair, M.F. Shakir, A. Afzal, Z.A. Rehan, Y. Nawab, *J. Supercond. Nov. Magn.* **34**, 201–210 (2021). <https://doi.org/10.1007/s10948-020-05669-x>
42. S.K. Ghosh, T.K. Das, S. Ganguly, S. Paul, K. Nath, A. Katheria, T. Ghosh, S.N. Chowdhury, N.C. Das, *Compos. Part. A* (2022). <https://doi.org/10.1016/j.compositesa.2022.107118>
43. J. Yan, Y. Huang, X. Liu, X.X. Zhao, T. Li, Y. Zhao, P. Liu, C. Dong, L. Zhang, K. Zhu, *Polymers* **14**, 5139 (2022). <https://doi.org/10.3390/polym14235139>
44. E.O. N.Ramdani, M.S. Mokhnache, N.A. Razali, M. Deradji, M. Maamar, *J. Compos. Mater.* **57**(17), 2703–2715 (2023). <https://doi.org/10.1177/00219983231179107>
45. S.D.A.S. Ramoa, G.M.O. Barra, C. Merlini, S. Livi, B.G. Soares, A. Pegoretti, *Polym. Adv. Technol.* **29**, 1377–1384 (2018). <https://doi.org/10.1002/pat.4249>
46. P. Gahlouta, V. Choudhary, *Synth. Metal.* **266**, 116414 (2020). <https://doi.org/10.1016/j.synthmet.2020.116414>
47. J.F. Pires Neto, L.F. Calheiro Souto, A. Anjos Silva, G.M. Oliveira, M.F. Barra, B.G. Naccache, A. Soares, S. Sirqueira, *J. Vinyl. Add. Technol.* **26**, 348–3530 (2020)
48. A. Kaynak, A.S. Mohan, J. Unsworth, R. Clout, *J. Mater. Sci. Lett.* **13**, 1121–1123 (1994)
49. W.B. Weir, *IEEE. Org.* **62**, 33–36 (1974). <https://doi.org/10.1109/Proc.1974.9382>
50. I. Ebrahimi, M.P. Gashti, *J. Phys. Chem. Solid.* **118**, 80–87 (2018)

Publisher's Note Springer Nature remains neutral with regard to jurisdictional claims in published maps and institutional affiliations.

Springer Nature or its licensor (e.g. a society or other partner) holds exclusive rights to this article under a publishing agreement with the author(s) or other rightsholder(s); author self-archiving of the accepted manuscript version of this article is solely governed by the terms of such publishing agreement and applicable law.